10-15-2012

Quantifying the CDK inhibitor VMY-1-103's activity and tissue levels in an in vivo tumor model by LC-MS/MS and by MRI.

Paul Sirajuddin
Lombardi Comprehensive Cancer Center, Department of Oncology, Georgetown University Medical Center

Sudeep Das
Department of Chemistry, Georgetown University

Lymor Ringer
Lombardi Comprehensive Cancer Center, Department of Oncology, Georgetown University Medical Center

Olga C Rodriguez
Lombardi Comprehensive Cancer Center, Department of Oncology, Georgetown University Medical Center

Angiela Sivakumar
Lombardi Comprehensive Cancer Center, Department of Oncology, Georgetown University Medical Center

See next page for additional authors

Cell Cycle 11:20, 3801–3809; October 15, 2012; © 2012 Landes Bioscience

Quantifying the CDK inhibitor VMY-1-103's activity and tissue levels in an in vivo tumor model by LC-MS/MS and by MRI

Paul Sirajuddin,[1,†] Sudeep Das,[2,†] Lymor Ringer,[1] Olga C. Rodriguez,[1] Angiela Sivakumar,[1] Yi-Chien Lee,[1] Aykut Üren,[1] Stanley T. Fricke,[3] Brian Rood,[3] Alpay Ozcan,[4] Sean S. Wang,[1] Sana Karam,[5] Venkata Yenugonda,[6] Patricia Salinas,[1] Emanuel Petricoin III,[7] Michael Pishvaian,[1] Michael P. Lisanti,[8] Yue Wang,[4,9] Richard Schlegel,[1,10] Bahram Moasser[2] and Chris Albanese[1,10,*]

[1]Lombardi Comprehensive Cancer Center and Department of Oncology; Georgetown University Medical Center; Washington, DC USA; [2]Department of Chemistry; Georgetown University; Washington, DC USA; [3]Children's National Medical Center; Washington, DC USA; [4]Department of Physics; Virginia Tech; Arlington, VA USA; [5]Department of Radiation Biology; Georgetown University Medical Center; Washington, DC USA; [6]Drug Discovery Program; Georgetown University Medical Center; Washington, DC USA; [7]Center for Applied Proteomics and Molecular Medicine; School of Systems Biology; George Mason University; Manassas, VA USA; [8]Department Stem Cell Biology; Kimmel Cancer Center; Thomas Jefferson University; Philadelphia, PA USA; [9]Bradley Department of Electrical and Computer Engineering; Virginia Tech; Arlington, VA USA; [10]Department of Pathology; Georgetown University Medical Center; Washington, DC USA

[†]These authors contributed equally to this work.

Keywords: CDK inhibitor, tandem mass spectrometry, animal models, prostate, medulloblastoma, MRI, MR-spectroscopy

The development of new small molecule-based therapeutic drugs requires accurate quantification of drug bioavailability, biological activity and treatment efficacy. Rapidly measuring these endpoints is often hampered by the lack of efficient assay platforms with high sensitivity and specificity. Using an in vivo model system, we report a simple and sensitive liquid chromatography-tandem mass spectrometry assay to quantify the bioavailability of a recently developed novel cyclin-dependent kinase inhibitor VMY-1-103, a purvalanol B-based analog whose biological activity is enhanced via dansylation. We developed a rapid organic phase extraction technique and validated wide and functional VMY-1-103 distribution in various mouse tissues, consistent with its enhanced potency previously observed in a variety of human cancer cell lines. More importantly, in vivo MRI and single voxel proton MR-Spectroscopy further established that VMY-1-103 inhibited disease progression and affected key metabolites in a mouse model of hedgehog-driven medulloblastoma.

Introduction

The development of new small-molecule inhibitors for clinical anticancer use has gained increased attention because of the central role that protein kinases play in cellular proliferation and cell division. Many proteins have been identified as potential targets of small-molecule inhibition to affect therapeutic intervention, including the Rb/CDK4 complex, based on its central role in cell cycle regulation,[1] components of the PI3Kinase pathway,[2] as well as the heat shock protein HSP90 in melanoma[3] and Poly (ADP-ribose) polymerase to sensitize brain tumors to radiation treatment.[4] However, establishing the bioavailability of new compounds can be confounded by a lack of rapid and robust assays. For example, techniques such as radioimmunoassays, binding assays[5] and HPLC separation[6,7] can frequently fail to meet the requirements of throughput and accuracy, as they may lack sensitivity or specificity, may not be quantitative or may be time consuming. Similarly, documenting in vivo tumor responsiveness is often very difficult due to, among other reasons, the anatomic location of the tumor in organs such as the liver, prostate and brain, and monitoring surrogate tissues such as peripheral blood mononuclear cells does not always reflect antitumor activity.

The purvalanols are members of the 2,6,9-trisubstituted purine group of cyclin-dependent kinase (CDK) inhibitors, which are generally well tolerated in vivo.[8] We have previously established that VMY-1-103 (VMY), a dansylated analog of purvalanol B (PVB), induced apoptosis at least 10-fold more potently in vitro than PVB in human prostate cancer,[9] medulloblastoma (MB)[10] and breast cancer[11] cell lines. Dansylation of compounds is known for its ability to enhance detection by mass spectrometry,[12] suggesting mass spectrometry could be used to evaluate the distribution of VMY in both serum and tissue samples when administered in vivo.

We have previously described the use of magnetic resonance imaging (MRI) and the ND2-SmoA1 preclinical medulloblastoma (MB) mouse model for preclinical testing of small-molecule compounds for the treatment of MB,[13] and we have used anatomical MRI and proton MR-spectroscopy (^{1}H-MRS) to

*Correspondence to: Chris Albanese; Email: albanese@georgetown.edu
Submitted: 07/22/12; Revised: 08/26/12; Accepted: 08/27/12
http://dx.doi.org/10.4161/cc.21988

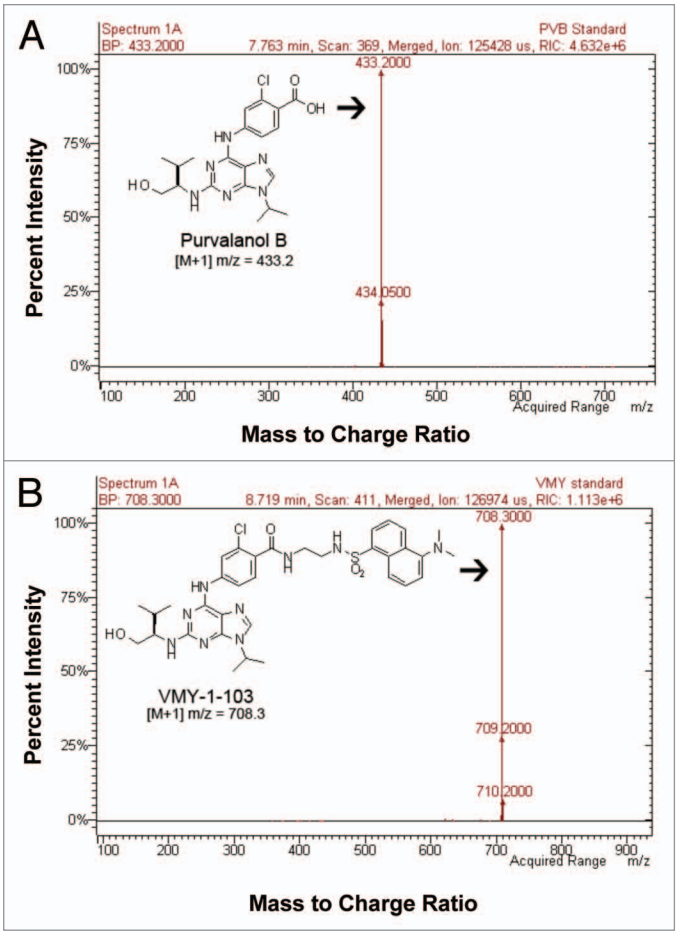

Figure 1. Detection of (A) PVB (433.2 m/z, 7.7 min) and (B) VMY (708.3 m/z, 8.7 min) by LC-MS/MS in the positive mode.

follow tumorigenesis in mouse models of prostate,[14] breast[15] and gastric[16] cancers. In the present study, we evaluated VMY's bioavailability and efficacy in normal and ND2-SmoA1 mice using LC-MS/MS and MRI.

Herein, we provide the methodologies necessary to perform rapid tissue extraction of VMY and PVB using a phase separation technique and coupled this to detection by liquid chromatography tandem mass spectrometry (LC-MS/MS). Through applying area under the curve (AUC) analyses, quantification of VMY in target tissues, such as brain, prostate, blood and urine, was also achieved. In addition, longitudinal MRI and single voxel proton MR-spectroscopy (^{1}H-MRS) enabled an in vivo visualization of VMY's impact on MB, establishing that VMY was able to affect changes in tumor metabolism and block disease progression in the ND2-SmoA1 medulloblastoma model.

Results

To establish the use of LC-MS/MS as a quantitative method for measuring these compounds, direct injections of VMY and PVB were performed in the positive mode and yielded a base peak of 433.2 m/z (M+1) for PVB, as predicted by the molecular mass (**Fig. 1A**), and a base peak at 708.3 m/z (M+1) for VMY, as predicted (**Fig. 1B**). The peak intensities of PVB and VMY occurred at 7.7 and 8.7 min, respectively. Standard curves for VMY and PVB were run on serial dilutions in methanol as described in the Methods (**Fig. 2**). Each standard curve was run in triplicate. Both calibration curves showed high linearity with VMY having a linear range of 0.00018–14.0 μM and PVB having a linear range of 0.0024–2.0 μM with R-squared values of 0.997 and 0.995, respectively.

The lowest limit of quantitation (LLOQ) was defined as the lowest concentration at which the MS signal was equal to 20 kilocounts, or the signal to noise ratio was greater than 10. Using these values and the data from the calibration curves the calculated LLOQ values for VMY and PVB were projected to be 0.15 nM and 2.2 nM, respectively.

We next determined the empirical limit of detection. Limiting dilutions of PVB and VMY were performed to define the limits of detection for both compounds, and area under the curve analyses (AUC) were performed to quantify the sample. The observed LLOQ values of VMY and purvalanol B were 0.18 nM for VMY and 2.4 nM for PVB (**Fig. 3**) and were in agreement with the projected values of 0.15 nM for VMY and 2.2 nM for PVB. These experiments establish that dansylation both increased measurement sensitivity by approximately 15-fold at the lowest limits of detection and significantly increased the linear range of VMY quantification.

Effects of danyslation on solubility. Having developed an accurate and sensitive assay for VMY and PVB, we next addressed the effects that danyslation may have on the chemical characteristics of VMY. We previously established that VMY was significantly more effective than PVB in inducing cell cycle arrest and apoptosis in cancer cells[9-11] and hypothesized that the dansyl modification increased the VMYs lipophilicity, enhancing its ability to traverse the cell membrane. In order to quantify the lipid solubility of both VMY and PVB, we performed partition coefficient measurements, which quantifiy solubility in either an organic or aqueous phase. Using phosphate buffered saline and n-octanol and applying the LogD formula described in the Methods section, the partition coefficients of VMY and PVB at pH 7.4 were found to be 2.03 ± 0.02 (n = 3) and 0.15 ± 0.002 (n = 3), respectively, confirming the increased lipophilicity of VMY.

LC-MS/MS detection of VMY in mouse tissue. In order to perform calculations of the concentration of VMY or PVB contained within tissue fragments, the methodology for, and efficiency of, extraction of VMY and PVB from tissue was first established. Efficiencies of extraction were modeled by injecting 1.55 micromoles in 55 microliters of either compound into 108 μg fragments of fresh mouse spleen. The tissues were stored on ice for 60 min. The fragments were homogenization in water, and an organic phase extraction methodology using dichloromethane (DCM) was developed as described in the Methods section. Following the organic phase extraction and separation by centrifugation, the samples were lyophilized, resuspended in methanol and quantified by LC-MS/MS as described in the Methods section. Using this method, both compounds were equally recovered from tissue at an average of 97% efficiency (n = 3, not shown), establishing that the different LogD values for VMY and PVB

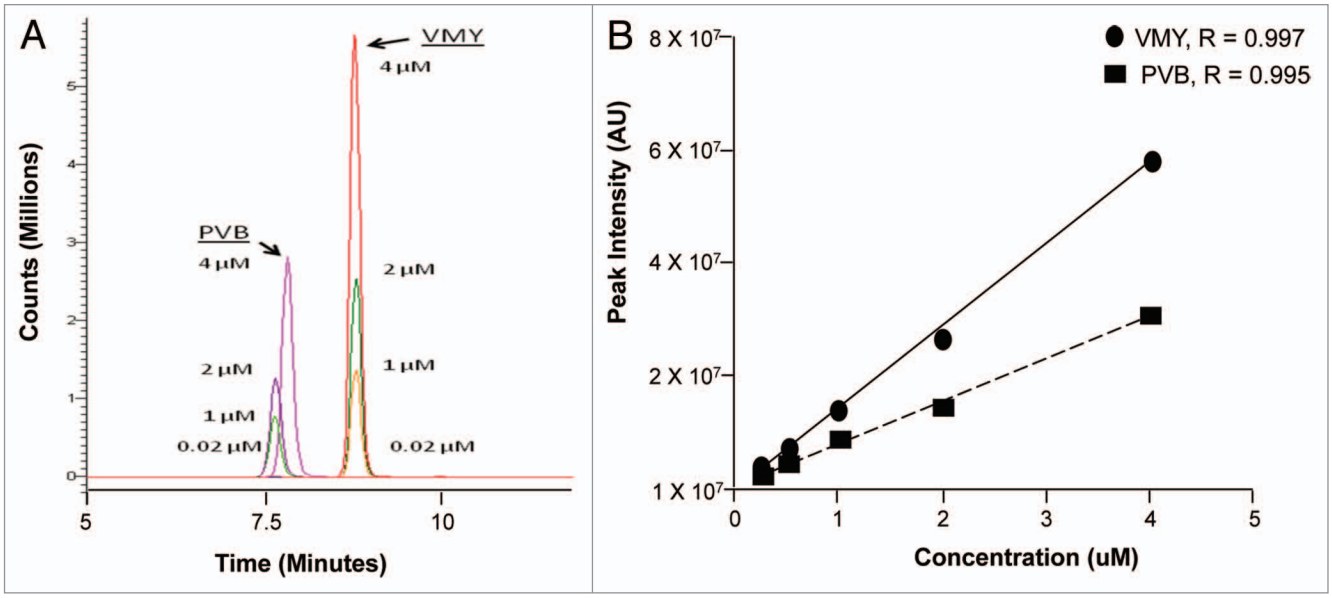

Figure 2. Calibration curves. (A) LC-MS/MS calibration curves of PVB (7.7 min) and VMY (8.7 min) at the concentrations shown. (B) Calibration curve calculations and R correlation coefficients for VMY and PVB.

do not adversely influence recovery of the compounds from tissue using the methods we developed.

For in vivo delivery experiments, mice were injected with either vehicle (peanut oil), VMY or PVB at 20 mg/kg. Tissues were collected at 1, 4 and 24 h after injection. Venous blood was collected from the heart. The excised tissues were weighed on an analytical balance, homogenized in water and processed as described in the Methods section. As an internal standard, 125 nanomoles of PVB was added to the VMY samples, followed by LC-MS/MS as described. Chromatograms from representative kidney samples are shown (**Fig. 4A**). The peak intensities occurred at 7.7 min for the PVB internal standard and 8.7 min for VMY, as expected. The kinetics and distribution of VMY in tissue are shown (**Fig. 5**). At 1 h post injection, VMY was easily detected in prostate, pancreas, fat, urine, serum and spleen. By 4 h, VMY was detected at its highest levels in these tissues and was also found in the kidney (**Fig. 5A**). At the 24 h time point, VMY was detectable in all tissues, except the spleen, at reduced levels vs. the 4 h time point (**Fig. 5A**). VMY was also administered at 20 mg/kg by oral gavage, and the highest amount of VMY was found in the kidney and serum at 1 h, and in the pancreas and spleen at 4 h, post-injection (**Fig. S1A**).

We next investigated the tissue distribution of PVB similarly administered at 20 mg/kg via intraperitoneal injection. PVB was detected in kidney, spleen, pancreas, prostate lung and serum (**Fig. 5B**). The overall tissue and serum levels of PVB, while lower than VMY (note differences in scale), were generally within the linear range of detection.

LC-MS/MS detection of VMY in brain tissue. Tissue samples from the normal cerebellum and cortex were excised from mice 4 hours after VMY injection. As with the other tissue samples, the brain samples were homogenized in water, extracted with DCM and analyzed by LC-MS/MS. While measurable amounts of PVB were not detected in the cortex or cerebellum (**Fig. 5C**), VMY at concentrations of 0.14 ± 0.05 uM and 0.53 ± 0.17 uM were found in the cerebellar and cortical tissue, respectively (**Fig. 5C**). Similar results were seen for VMY delivery to the brain following oral gavage (**Fig. S1B**).

We have previously used the the ND2-SmoA1 mouse model of human medulloblastoma (MB) to establish that subclinical doses of the FDA-approved antineoplastic compound arsenic trioxide were effective at treating MB in vivo.[13] Since VMY was present in the brain of normal mice with intact blood brain barriers (BBB), we investigated whether VMY could be found in the tumors of MB-bearing mice, which have a compromised BBB. ND2-SmoA1 mice with spontaneous tumors were identified by MRI, as previously described,[13] and the mice were treated with VMY as above. MB samples collected 4 hours after injection had an average VMY concentration of 0.5 ± 0.2 uM (**Fig. 5C**).

VMY decreases tumor growth and metabolism in the SmoA1 mouse model of MB. Since VMY was readily detectable in MB tumors, we performed longitudinal studies investigating the effect of VMY on tumor growth. Once tumors were detected by MRI, initial tumor volumes were established by manual segmentation. Animals were randomly chosen for intraperitoneal injections with either VMY (20 mg/kg as above) or vehicle (peanut oil), and the treatments performed three times per week for up to 12 weeks as an endpoint. There were no significant differences in tumor volume at initial diagnosis, ($p = 0.20$ using a one-tailed Mann-Whitney U test, $n = 6$, **Fig. 6A**), and no significant toxicities were observed during the study. Final tumor volumes were established by MRI followed by termination of the study. The average tumor volume as established by manual segmentation was 1.46 ± 1.21 mm^3 for control and 0.31 ± 0.25 mm^3 for VMY, which is statistically significant ($p = 0.03$, $n = 6$ mice in each group) using a one-tailed Mann-Whitney U test. The

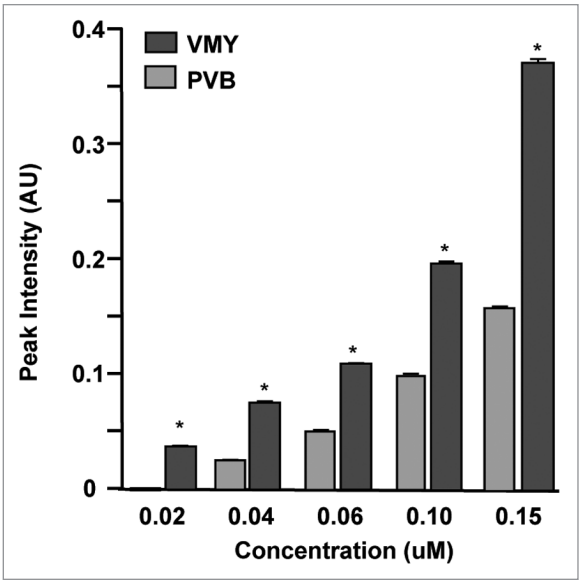

Figure 3. Limits of detection by LC-MS/MS. VMY and PVB at the concentrations shown and plotted against count intensities in arbitrary units (AU). Data are average ± standard deviation of n = 3 separate experiments. *, $p < 0.01$ vs. PVB using Student's t-test's

overall fold-increase in tumor volume from initial diagnosis to study termination was found to be 10.0 ± 3.6 (SEM)-fold in control animals vs. 3.74 ± 1.45 (SEM)-fold in VMY-treated animals, a statistically significant difference ($p = 0.014$, $n = 6$). Single voxel proton MR-spectroscopy (^{1}H-MRS) was used to interrogate tissue metabolism, as described in the Methods and in previous publications.[14,15] A representative example of voxel placement and the resulting ^{1}H-MR spectra is shown (**Fig. 6B**). The relative ratios of tumor metabolites relative to levels of total creatine (Cr) were derived following approximately 2 weeks of treatment. Creatine levels are relatively constant even under certain pathological conditions, and this marker is commonly utilized as an internal ^{1}H-MRS reference. The ^{1}H-MRS revealed that VMY treatment resulted in statistically significant increases in the ratios of Tau (taurine, $p = 0.024$, $n = 3$) to Cr and mI (myo-inositol, $p = 0.024$, $n = 3$) to Cr, using one-tailed Mann-Whitney U tests, with little to no changes in the Cho (choline) or NAA (N-acetyl-aspartate) to Cr ratios (**Fig. 6C**). Following termination of the study, histological and immunohistochemical analyses revealed an overall change in tumor architecture by VMY, including extensive areas containing cells with condensed or fragmented nuclei indicating cellular necrosis (**Fig. S2**). Using one-tailed Mann-Whitney U tests, VMY was found to induce significant increases in TUNEL-positive cells (8.9% ± 1.8 for VMY vs. 5.9% ± 0.5 for control, $p = 0.01$, **Fig. 6D**) and PCNA-positive cells (38.3% ± 12.4 for VMY vs. 13.3% ± 12.1 for control, $p = 0.025$, **Fig. 6D**), with concomitant decreases in nuclear cyclin D1 positivity (13.8% ± 4.0 for VMY vs. 33.1% ± 4.9 for control, $p = 0.024$, **Fig. 6D**). These data are consistent with VMY-induced apoptosis and cell cycle arrest in G_2/M[17] and consistent with VMY's effects on cell cycle progression and apoptosis in human medulloblastoma cell lines in vitro.[10]

Discussion

The ability to rapidly and accurately quantify the delivery of therapeutic compounds to target tissues is an important component of drug discovery as well as the preclinical testing of novel agents. Unfortunately, the assays used to perform these analyses are often complicated, time consuming and, in some cases, indirect. In the present study, we established a simplified methodology to quantify, VMY and PVB, members of the trisubstituted purine analog family of small-molecule inhibitors, from mouse serum. While we have shown that dansylation allows for the in vitro identification by fluorescence microscopy of prostate and medulloblastoma cells that contain VMY,[9,10] this fluorophore was insufficient for imaging or quantification of drug delivery in vivo (not shown). However, since dansylated compounds are readily detectable using mass spectrometry, our expectation was that VMY's dansyl group would enhance our ability to measure tissue distribution by LC-MS/MS. VMY's detection sensitivity was increased by nearly 15-fold at the lowest limits of detection, and overall sensitivity increased approximately 2-fold vs. PVB.

As shown in **Figure 2**, PVB and VMY have different column retention times. We took advantage of this chemical difference to overcome the need for performing total ion counts for quantification of VMY. By using multiple ion trapping, we were able to detect PVB and VMY individually in separate channels, allowing the use of PVB as an internal standard for VMY tissue quantification. One of the major challenges was developing a method to extract the small-molecule inhibitors from various tissues, including the blood, without significant sample loss or residual tissue fragmentation that could compromise the ability to perform spectrometry. We found that an aqueous tissue sonification followed by dichloromethane extraction and phase separation centrifugation, a procedure we developed, was superior to other methods, such as methanol and acetonitrile extraction and syringe-driven filtration (not shown). The dichloromethane extraction and centrifugation effectively forced hydrophilic cellular components, including tissue fragments, into the aqueous layer, while the hydrophobic VMY and PVB compounds were retained in the organic layer, allowing for quick and accurate collection without the need for filtering. In addition, neither VMY nor PVB were detected in the aqueous layer (**Fig. S3**), indicating that dichloromethane is an appropriate solvent, and extraction conditions provided for extremely efficient recovery of this class of compound. Although dichloromethane can be injected directly into the ESI ion trap, we found that evaporation of the DCM and resuspension in methanol yielded excellent reproducibility, possibly due to better ionization by methanol (not shown).

We had previously speculated that VMY's increased potency might be due in part to increased lipid partitioning provided by the dansyl group, allowing for better transport across the cell membrane.[9-11] We now show that VMY is significantly more lipid soluble than PVB and, consistent with this, we found VMY at higher overall amounts in the blood and tissues, such as prostate, which is one of the proposed target organs for VMY therapy. In addition, while VMY was consistently found in MB tumor samples, as anticipated, VMY was also present in the brain

samples of normal mice with intact BBBs. One of the challenges for developing drugs that are meant to target brain malignancies is documenting their ability to cross the BBB. Methodologies for delivering drugs to the brain have involved intrathecal administration, convection enhanced delivery via surgically implanted catheters, intra-arterial delivery, surgical implantation with drug impregnated discs as well as BBB disruptants such as bradykinin, mannitol or high intensity focused ultrasound.[18-20] More recently the BBB has been evaded by activating adenosine receptors,[21] further underscoring the need for compounds that contain an inherent ability to cross the BBB. Our data establish that delivery of purvalanol-based compounds across an intact BBB can be effectuated via dansylation, raising the possibility that similar modifications of other compounds may enhance the rational design of brain targeted therapeutics delivered intravenously, orally or via other routes, such as intranasal administration. Moreover, dansylation also served as an effective "tag," greatly increasing the measurement of drug via a rapid and sensitive mass spectrometry-based detection method. Such an approach could be useful in future studies, whereby biodistribution and detection are enhanced simultaneously with a single modification.

Finally, we have applied MRI and ^{1}H-MRS to non-invasively measure tumor responses to VMY. In addition to inhibiting tumor growth as measured by segmentation, ^{1}H-MRS established that the relative concentrations of taurine and myo-inositol were altered in tumors following treatment with VMY. Taurine has been found to play a variety of possible roles in the nervous system, including affecting osmoregulation, maintaining the integrity of the membrane, regulating calcium transport and homeostasis and, possibly, functioning as a neuroprotectant.[22] The increase in Tau seen following VMY treatment may be related to its osmoregulatory role, or perhaps it is in response to the increase in overall cellular apoptosis brought about by VMY. Myo-inositol is considered a marker of glial cells and changes in the levels of mI are associated with white matter diseases and grade II astrocytomas.[23] Additionally, mI is expected to be altered in response to damaged cellular membranes, and increased mI levels are also associated with inflammation, and the histological data from the mice confirms an increase in inflammation. Other key metabolites were not significantly affected. Choline levels are abundant in the MBs of this mouse model,[24] and studies have established that the levels of choline levels are relatively consistent both in brain tumors and in normal brain tissue,[25-27] and our data support these finding. N-acetylaspartate (NAA) is a marker of neuronal metabolism and the relative levels of NAA were unaffected by VMY treatment, suggesting that VMY did not have an overall adverse effect on the brain, as levels of NAA would be expected to change. Based on these data we believe that ^{1}H-MRS may be a more sensitive and therefore a more effective early measure of drug effectiveness than are changes in overall tumor volume, and additional studies are underway to explore this hypothesis.

The development of non-invasive imaging methods to measure responses to chemotherapy, combined with post-mortem data including drug bioavailability, histopathology and molecular analyses, performed in biologically relevant preclinical models will enhance our ability to investigate the applicability of new and existing drugs. Importantly, all of the methodological approaches we have described can be easily translated into clinical use, furthering our ability to predict tumor responsiveness in vivo and to accurately measure drug delivery and efficacy using biopsied tissue.

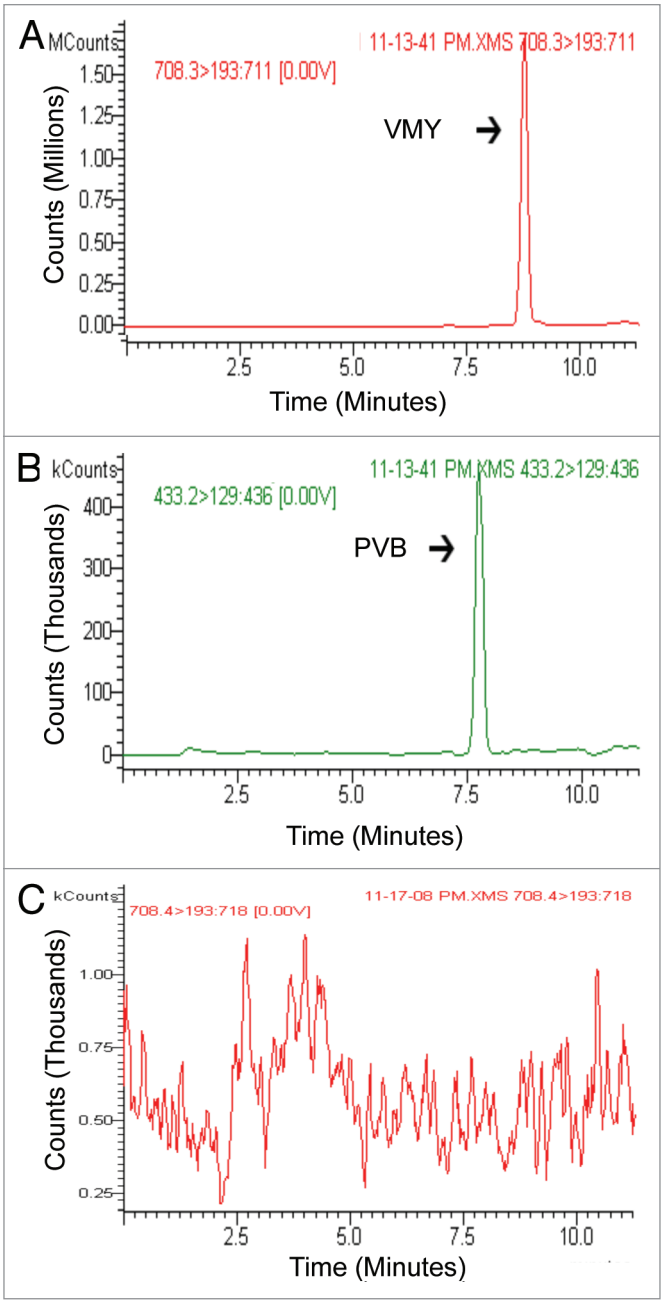

Figure 4. Measuring VMY or PVB in tissue samples. Representative dual ion LC-MS/MS tissue spectra from mice injected with (A) VMY, (B) PVB and (C) vehicle (peanut oil).

Methods and Materials

Chemicals. Purvalanol B (P5234) and Octanol (112615) were purchased from Sigma-Aldrich. HPLC grade methanol, HPLC

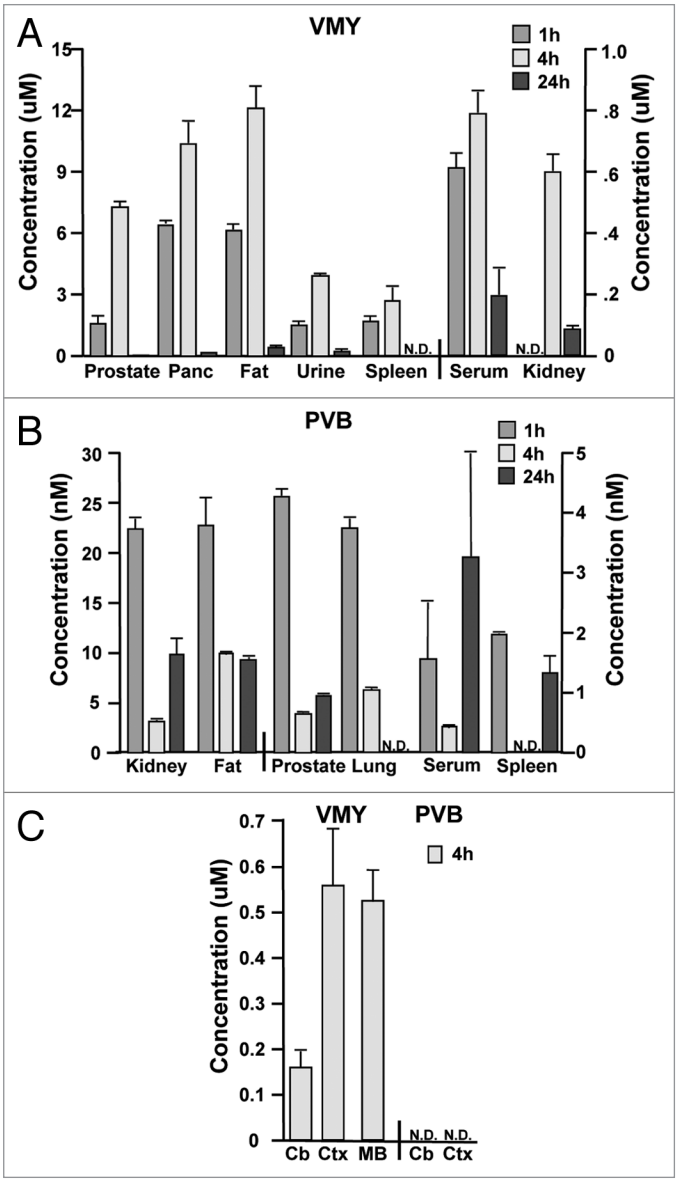

Figure 5. In vivo tissue delivery and quantification. Tissue samples were collected at the times shown from mice that received intraperitoneal injections of (A) 20 mg/kg VMY or (B) 20 mg/kg PVB (note: Y axis is micromolar in (A) vs. nanomolar in (B). (C) Brain tissue from mice injected with VMY or PVB. All data are average ± standard deviation of three separate samples. Panc, pancreas; Cb, cerebellum; Ctx, cortex; MB, medulloblastoma; N.D., not determinable (below levels of detection).

grade dichloromethane (DCM), HPLC grade water, phosphate buffered saline (PBS) pH 7.4 and formic acid were purchased from Fisher Scientific.

VMY-1-103 synthesis and purification. VMY-1-103 was synthesized as previously described. Briefly, starting from commercially available 2-fluoro-6-chloropurine, standard N-9 alkylation with 2-propanol under Mitsunobu conditions gave 2-fluoro-6-chloro-9H-isopropylpurine. The 6-position was substituted with dansyl ethylenediamine, followed by substitution at the 2-position (R)-valinol, yielding VMY-1-103.[11]

Table 1. Liquid chromatography tandem mass spectrometry

Mass spectrometer parameter	
Spray chamber temperature	50°C
Nebulizer gas	Nitrogen
Nebulizer pressure	35 p.s.i.
Drying gas temperature	350°C
Drying gas pressure	18 p.s.i.
Needle voltage (+)	5000 V
Sprayshield voltage (+)	600 V
Data rate	0.30 Hz

SmoA1-ND2 preclinical mouse model. We have recently described the use of the ND2-SmoA1 preclinical medulloblastoma (MB) mouse model (a generous gift from James Olsen) for preclinical testing of small molecule compounds for treatment of MB.[13] Briefly, this model contains the SmoA1 constitutively active point mutation of the Smoothened transmembrane receptor under the control of the *NeuroD2* mouse promoter, resulting in spontaneous cerebellar medullulоblastoma at 3–4 mo of age. Normal, nontransgenic C57Bl6 mice were also used for in vivo drug studies. All mice were kept, handled and euthanized in accordance with the Georgetown University Division of Comparative Medicine's ethics guidelines and conditions. Mice were genotyped for the SmoA1 transgene as previously described.[13] VMY or PVB were solubilized in peanut oil and were administered at 20 mg/kg. For timepoint studies, mice were sacrificed 1 h, 4 h and 24 h after injection. Serum and tissue were collected at necropsy. Mice with medulloblastoma were identified by MRI as previously reported[13] and described below.

MRI. All MRI procedures were performed on the 20 cm bore, 7T Bruker horizontal magnet running Paravision 5 (Bruker) in the Georgetown-Lombardi Preclinical Research Imaging Laboratory. Quantitative tumor volumetric analyses were performed essentially as previously described.[28] Mice were anesthetized using 1.5% isoflurane and 30% nitrous oxide and positioned inside the magnet using a custom-designed animal management system with temperature and respiration control,[28] which was with further adapted to accept a Bruker 4 channel brain array coil. The imaging protocol used for anatomical evaluation was a T2-weighted RARE (rapid acquisition with relaxation enhancement) with the following parameters: matrix: 256 × 256, TR: 4660 ms, TE: 36 ms, spatial resolution: 137 μm/pixel and slice thickness: 0.5 mm. Quantitative tumor volumetric analyses were performed as previously described.[14]

MRS. Single voxel proton MRS was performed using PRESS (Position Resolved Spectroscopy Sequence), essentially as previously described.[14,15] Briefly, parameters of the MRS sequence are: TE: 20 ms, TR: 2500 ms, averages: 1,024, spectral width of 4 kHz, and 2,048 complex data points and 6 Hz line broadening, using a voxel of 1–2 mm on edge located entirely in tumor areas avoiding contamination from normal brain tissue. The voxel was positioned using the RARE anatomical image as a locator scan. Quantification of neurochemicals was performed using the Bruker software program TOPSPIN. When necessary, corrections were made for voxel volume related to the size, shape and location of the tumor. For comparison of in vivo MRS data, creatine was used as the internal standard. Statistical analyses

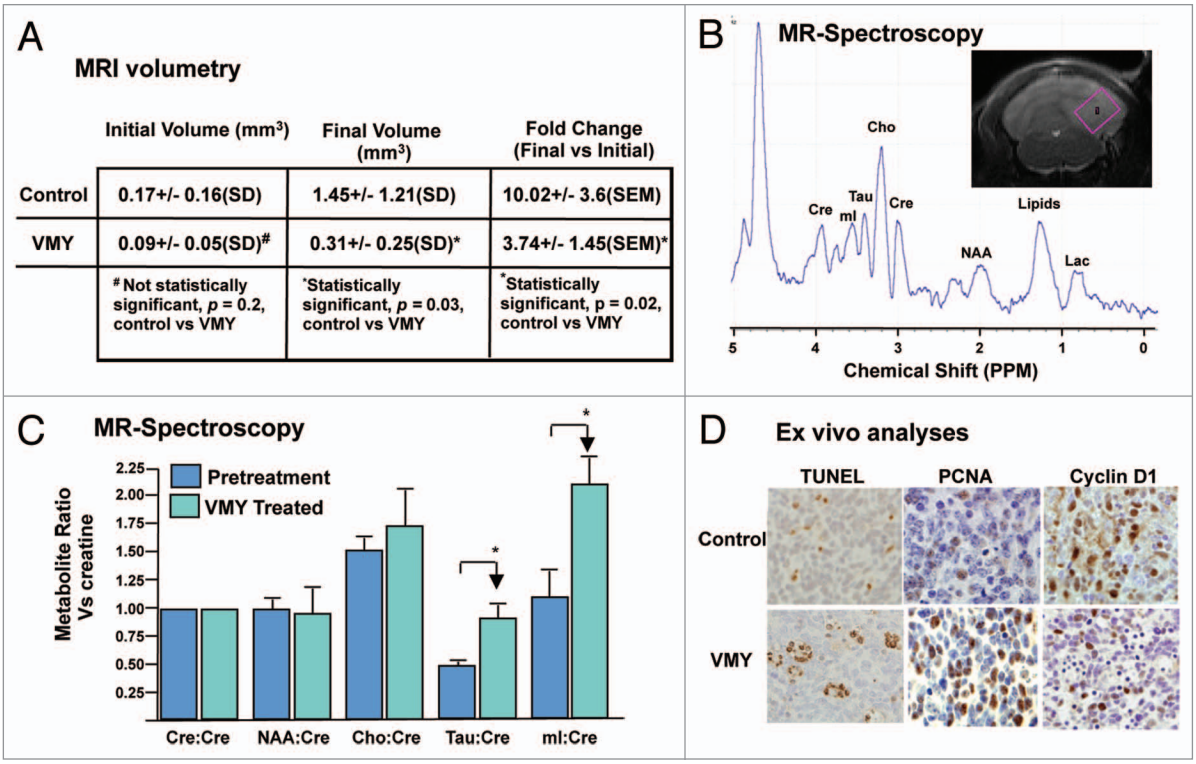

Figure 6. Effect of VMY on tumor growth and metabolism. (A) Initial and final tumor volumes as measured by MRI. Data are average ± of either standard deviation (SD) or standard error of the mean (SEM) of n = 6 mice in each group. (B) Representative voxel placement and in vivo MR-spectral profile of MB. (C) Effect of VMY on metabolite ratios. Metabolite ratios were established relative to creatine (Cr). (D) TUNEL, PCNA and cyclin D1 immunohistochemical staining of control and VMY-treated MB samples from the mice in (A–C). Abbreviations: mm^3, cubic millimeters; Cre, creatine; Tau, taurine; NAA, N-acetyl-apartate; PPM, parts per million. Data are average ± standard deviation of n = 3 mice asterisk, p < 0.05 using one-tailed Mann Whitney U-tests.

were performed using the Mann-Whitney U test due to the small sample size, and actual p values are shown. Tissue and serum samples were harvested at the termination of the study and either immediately fixed in formalin or processed for mass spectrometry.

LC-MS/MS detection of compounds. *Mass spectrometry.* Varian workstation software version 6.9.1 was used operate the LC-mass spectrometer and autosampler. Drug detection and quantification was performed using a Varian 500 ion trap LC-MS/MS. Ionization was done using electrospray interface (ESI) in the positive mode with operating conditions summarized in **Table 1**. VMY (exact mass 707.28 amu) was detected as an (M+1) ion at 708.35 m/z. PVB (exact mass 432.17) was detected as an (M+1) ion at 433.21m/z. Conditions for detection of VMY and PVB are summarized in **Table 2**. Both VMY and PVB were detected simultaneously in a single run using two different channels.

Liquid chromatography. Varian 212-LC chromatography pumps were used with a Pursuit XRs 3 μm C18 100X2.0mm column, Restek Ultra 5 μm 20X2.1 mm guard cartridge. Water with 0.1% formic acid and methanol with 0.1% formic acid were passed through though pumps A and B, respectively. The pump program is summarized in **Table 3**. Columns were equilibrated for 15 min between automated runs with 7 min for ramp and 8 min for hold which was found to be optimum for this system.

Autosampler. A Varian Prostar 410 autosampler was used for automation purposes. 10–20 μL injections were done using partial loop fill technique for maximum reproducibility.

Sample preparation. Fresh tissue samples were resuspended in 80 μL of methanol and transferred to 0.25 mL glass conical inserts with poly-support springs (VWR 46610–762) inside of Snap-vials (National Scientific) and injected using partial-loop uL injection. Standard curves were generated using serial dilutions of stock VMY and PVB made in methanol at concentrations of 4, 2, 1, 0.5, 0.25, 0.02 μM, and analyzed by LC-MS/MS using the described method above. The R-values for VMY and PVB were calculated using GraphPad Prism software by plotting the linear regression against the calibration curve intensity values.

Statistical and empirical limit of quantitation (LOQ). Ten blank controls with a matrix identical to the experimental samples were analyzed by LC-MS/MS, and the mean blank signal value and SD were calculated. The statistical LOQ $(S_A)_{LOQ}$ was calculated from the mean blank value plus 10 standard deviations and summarized in the equation below, where $(S_A)_{LOQ}$ is the signal at the limit of quantitation, (S_{reag}) is the value of the average blank signal, σ is the standard deviation, and z is the significance level (set to 10 for the strictest criteria). The lowest limit of quantitation (LLOQ) is the lowest concentration in the calibration curve at which the $(S_A)_{LOQ}$ signal was equal to 20 kilocounts or the signal to noise ratio greater than 10. $(SA)_{LOQ} = S_{reag} + z\sigma_{reag}$.

Table 2. Mass spectrometry parameters for detecting VMY and PVB

Isolation window (m/z)	Waveform type	Storage level (m/z)	Excitation amplitude (m/z)	Ion start mass (m/z)	Ion end mass (m/z)	RF loading (%)	Capillary voltage (Volts)	High/low offset (m/z)	Excitation time (msecs)	Modulate Rf	Num freq.
VMY: 3.0	Resonant	193.1	0.0	193	711	80	100	0.0	30.0	Yes	0.0
PVB: 3.0	Resonant	129.0	0.0	129	436	64	110	0.0	30.0	Yes	0.0

Table 3. Pump program

Time (min)	%A	%B	Flow rate μl/min	Pressure (psi)
0:00	50	50	200	2340
10:00	0.0	100	200	-
15:00	0.0	100	200	1020

Quantification of VMY and PVB. The quantification of VMY and PVB in tissue was performed by using Area Under the Curve analysis (AUC) by integrating the peak intensity curve derived from LC-MS/MS using MS Data Viewer 6.9.1 software (Varian, Inc.). For tissue delivery analyses, each VMY sample was normalized using the internal standard and the total quantity of VMY was calculated by comparing the AUC of each normalized sample to the VMY calibration curve. Statistical significances calculations were performed using Student's t-tests

Isolation of VMY and PVB from tissue by phase separation. VMY or PVB was isolated from tissues using the following method. Mouse tissues, removed of any adherent liquid or moisture, were weighed on an analytical balance and individually placed in 2.0 mL Eppendorf tubes. 600 μL of HPLC grade distilled deionized H_2O was added, and the tissues were homogenized on ice using an OMNI Tissue Homogenizer (TH-115) equipped with two-piece OmniTip (3750H) at 35,000 rpm in three 45 sec bursts, incubating the sample on ice for 2 min between each burst. Next, 600 μL of HPLC grade dichloromethane (DCM, Fisher Scientific) was added to the homogenized sample, and the tube was vortexed for 1 minute and incubated on ice for 2 h. The sample was centrifuged at 14,000 rpm using an Eppendorf 5415R refrigerated centrifuge at 4°C for 20 min, resulting in a biphasic solution comprised of an aqueous layer with tissues debris and a clear DCM layer. The organic layer containing the VMY or PVB and the aqueous phases were collected separately in fresh tubes. This extraction process was repeated twice by adding an additional 600 μL of DCM to the original dH20 and tissue and re-extracting to obtain the maximum recovery. The DCM and aqueous layers from all three extractions were lyophilized to dryness and stored at -20°C. A modified procedure was performed to isolate VMY or PVB from the circulation, in which 30 μL of serum was aliquoted into 600 μL of HPLC grade dH20, and the DCM extraction procedure was performed without sonication. To validate that DCM extraction effectively extracted VMY and PVB from the tissue and aqueous phase, the aqueous fraction was subjected to LC-MS/MS and neither VMY nor PVB was found (**Fig. S3**).

For quantification of VMY across multiple experiments, 125 nanomoles of PVB was added as an internal standard to each sample prior to LC-MS/MS analysis.

Octanol-PBS partition coefficient (logD). The octanol and phosphate-buffered saline (PBS, pH 7.4) partition coefficient (logD) was determined using the traditional shake flask method[29,30] at 37°C. In a 4 mL vial, 1 mg of each test compound was weighed and dissolved in 1 mL of octanol-pre-saturated PBS, which was then shaken with 1 mL of PBS-pre-saturated octanol for 24 h at 37°C. The velocity of shaking was carefully chosen to prevent emulsion formation while allowing thorough mixing. After 24 h, the two phases were separated by centrifuging at 10,000 rpm for 10 min, and each layer was transferred into separate vials. The individual samples were injected into an LC-MS/MS to detect the quantity of the specified compound in each layer. The peak intensity value was used to calculate the area under the curve (AUC). The partition coefficients at pH 7.4 ($LogD_{7.4}$) of VMY and PVB were calculated using the AUC of the peak intensity and employing the equation: LogD7.4 = Log10(AUC_{oct}/injection volume of octanol phase) /(AUC_{buffer}/injection volume of buffer phase).

Immunohistochemical staining. Immunohistochemical staining was performed on prostate tissue as previously described.[13,31-34] The slides were blocked for 20 min and incubated overnight at 4°C with the primary antibody. Detection was performed as previously described.[13,31-34] Because of the small sample size statistical analyses were performed using the Mann-Whitney U test and actual p values are shown.

Disclosure of Potential Conflicts of Interest

A patent application has been filed by Georgetown University on the behalf of one of the inventors, Yenugonda, who is listed as an author on this article. All other authors declare no conflict of interest.

Acknowledgments

We would like to thank the Georgetown-Lombardi Preclinical Imaging Research laboratory for imaging the medulloblastoma mouse model and Dr. Gary Van Berkel for useful discussions on dansylation and mass spectrometry. The MRI was performed in the Lombardi Comprehensive Cancer Center's Preclinical Research Imaging Laboratory and the tissue sectioning and staining was performed in the Lombardi Comprehensive Cancer Center's Histology and Tissue Shared Resource. This work was supported by P30 CA51008 (Weiner), R01CA129003 (C.A.) and ABC2 (C.A.).

Supplemental Material

Supplemental material may be downloaded here:
www.landesbioscience.com/journals/cc/article/21988/

References

1. Paternot S, Bockstaele L, Bisteau X, Kooken H, Coulonval K, Roger PP. Rb inactivation in cell cycle and cancer: the puzzle of highly regulated activating phosphorylation of CDK4 versus constitutively active CDK-activating kinase. Cell Cycle 2010; 9:689-99; PMID:20107323; http://dx.doi.org/10.4161/cc.9.4.10611.
2. Garrett JT, Chakrabarty A, Arteaga CL. Will PI3K pathway inhibitors be effective as single agents in patients with cancer? Oncotarget 2011; 2:1314-21; PMID:22248929.
3. Beloueche-Babari M, Arunan V, Jackson LE, Perusinghe N, Sharp SY, Workman P, et al. Modulation of melanoma cell phospholipid metabolism in response to heat shock protein 90 inhibition. Oncotarget 2010; 1:185-97; PMID:21037799.
4. van Vuurden DG, Hulleman E, Meijer OL, Wedekind LE, Kool M, Witt H, et al. PARP inhibition sensitizes childhood high grade glioma, medulloblastoma and ependymoma to radiation. Oncotarget 2011; 2:984-96; PMID:22184287.
5. You AJ, Jackman RJ, Whitesides GM, Schreiber SL. A miniaturized arrayed assay format for detecting small molecule-protein interactions in cells. Chem Biol 1997; 4:969-75; PMID:9427662; http://dx.doi.org/10.1016/S1074-5521(97)90305-7.
6. Routledge C, Marsden CA. Recent advances in high-performance liquid chromatographic analysis of small molecules. Application of high-performance liquid chromatography with electrochemical detection to the study of neurotransmitters in vivo. Biochem Soc Trans 1985; 13:1058-61; PMID:2419180.
7. Konsoula R, Jung M. In vitro plasma stability, permeability and solubility of mercaptoacetamide histone deacetylase inhibitors. Int J Pharm 2008; 361:19-25; PMID:18562136; http://dx.doi.org/10.1016/j.ijpharm.2008.05.001.
8. Ghosh JC, Altieri DC. Activation of p53-dependent apoptosis by acute ablation of glycogen synthase kinase-3beta in colorectal cancer cells. Clin Cancer Res 2005; 11:4580-8; PMID:15958644; http://dx.doi.org/10.1158/1078-0432.CCR-04-2624.
9. Ringer L, Sirajuddin P, Yenugonda VM, Ghosh A, Divito K, Trabosh V, et al. VMY-1-103, a dansylated analog of purvalanol B, induces caspase-3-dependent apoptosis in LNCaP prostate cancer cells. Cancer Biol Ther 2010; 10:320-5; PMID:20574155; http://dx.doi.org/10.4161/cbt.10.4.12208.
10. Ringer L, Sirajuddin P, Heckler M, Ghosh A, Suprynowicz F, Yenugonda VM, et al. VMY-1-103 is a novel CDK inhibitor that disrupts chromosome organization and delays metaphase progression in medulloblastoma cells. Cancer Biol Ther 2011; 12:818-26; PMID:21885916; http://dx.doi.org/10.4161/cbt.12.9.17682.
11. Yenugonda VM, Deb TB, Grindrod SC, Dakshanamurthy S, Yang Y, Paige M, et al. Fluorescent cyclin-dependent kinase inhibitors block the proliferation of human breast cancer cells. Bioorg Med Chem 2011; 19:2714-25; PMID:21440449; http://dx.doi.org/10.1016/j.bmc.2011.02.052.
12. Dalvie DK, O'Donnell JP. Characterization of polar urinary metabolites by ionspray tandem mass spectrometry following dansylation. Rapid Commun Mass Spectrom 1998; 12:419-22; PMID:9586229; http://dx.doi.org/10.1002/(SICI)1097-0231(19980430)12:8<419::AID-RCM176>3.0.CO;2-S.
13. Beauchamp EM, Ringer L, Bulut G, Sajwan KP, Hall MD, Lee YC, et al. Arsenic trioxide inhibits human cancer cell growth and tumor development in mice by blocking Hedgehog/GLI pathway. J Clin Invest 2011; 121:148-60; PMID:21183792; http://dx.doi.org/10.1172/JCI42874.
14. Fricke ST, Rodriguez O, Vanmeter J, Dettin LE, Casimiro M, Chien CD, et al. In vivo magnetic resonance volumetric and spectroscopic analysis of mouse prostate cancer models. Prostate 2006; 66:708-17; PMID:16425198; http://dx.doi.org/10.1002/pros.20392.
15. Sakamaki T, Casimiro MC, Ju X, Quong AA, Katiyar S, Liu M, et al. Cyclin D1 determines mitochondrial function in vivo. Mol Cell Biol 2006; 26:5449-69; PMID:16809779; http://dx.doi.org/10.1128/MCB.02074-05.
16. Pollock CB, Rodriguez O, Martin PL, Albanese C, Li X, Kopelovich L, et al. Induction of metastatic gastric cancer by peroxisome proliferator-activated receptordelta activation. PPAR Res 2011; 2010:571783.
17. Kawabe T, Suganuma M, Ando T, Kimura M, Hori H, Okamoto T. Cdc25C interacts with PCNA at G2/M transition. Oncogene 2002; 21:1717-26; PMID:11896603; http://dx.doi.org/10.1038/sj.onc.1205229.
18. Black KL, Ningaraj NS. Modulation of brain tumor capillaries for enhanced drug delivery selectively to brain tumor. Cancer Control 2004; 11:165-73; PMID:15153840.
19. Joshi S, Ergin A, Wang M, Reif R, Zhang J, Bruce JN, et al. Inconsistent blood brain barrier disruption by intraarterial mannitol in rabbits: implications for chemotherapy. J Neurooncol 2011; 104:11-9; PMID:21153681; http://dx.doi.org/10.1007/s11060-010-0466-4.
20. McDannold N, Vykhodtseva N, Hynynen K. Blood-brain barrier disruption induced by focused ultrasound and circulating preformed microbubbles appears to be characterized by the mechanical index. Ultrasound Med Biol 2008; 34:834-40; PMID:18207311; http://dx.doi.org/10.1016/j.ultrasmedbio.2007.10.016.
21. Carman AJ, Mills JH, Krenz A, Kim DG, Bynoe MS. Adenosine receptor signaling modulates permeability of the blood-brain barrier. J Neurosci 2011; 31:13272-80; PMID:21917810; http://dx.doi.org/10.1523/JNEUROSCI.3337-11.2011.
22. Wu JY, Prentice H. Role of taurine in the central nervous system. J Biomed Sci 2010; 17(Suppl 1):S1; PMID:20804583; http://dx.doi.org/10.1186/1423-0127-17-S1-S1.
23. Candiota AP, Majós C, Julià-Sapé M, Cabañas M, Acebes JJ, Moreno-Torres A, et al. Non-invasive grading of astrocytic tumours from the relative contents of myo-inositol and glycine measured by in vivo MRS. JBR-BTR 2011; 94:319-29; PMID:22338386.
24. Hekmatyar SK, Wilson M, Jerome N, Salek RM, Griffin JL, Peet A, et al. ^{1}H nuclear magnetic resonance spectroscopy characterisation of metabolic phenotypes in the medulloblastoma of the SMO transgenic mice. Br J Cancer 2010; 103:1297-304; PMID:20842126; http://dx.doi.org/10.1038/sj.bjc.6605890.
25. McLean MA, Sun A, Bradstreet TE, Schaeffer AK, Liu H, Iannone R, et al. Repeatability of edited lactate and other metabolites in astrocytoma at 3T. J Magn Reson Imaging 2012; 36:468-75; PMID:22535478; http://dx.doi.org/10.1002/jmri.23673.
26. Saraswathy S, Crawford FW, Lamborn KR, Pirzkall A, Chang S, Cha S, et al. Evaluation of MR markers that predict survival in patients with newly diagnosed GBM prior to adjuvant therapy. J Neurooncol 2009; 91:69-81; PMID:18810326; http://dx.doi.org/10.1007/s11060-008-9685-3.
27. Howe FA, Opstad KS. 1H MR spectroscopy of brain tumours and masses. NMR Biomed 2003; 16:123-31; PMID:12884355; http://dx.doi.org/10.1002/nbm.822.
28. Fricke ST, Vink R, Chiodo C, Cernak I, Ileva L, Faden AI. Consistent and reproducible slice selection in rodent brain using a novel stereotaxic device for MRI. J Neurosci Methods 2004; 136:99-102; PMID:15126050; http://dx.doi.org/10.1016/j.jneumeth.2004.01.003.
29. Avdeef A, Testa B. Physicochemical profiling in drug research: a brief survey of the state-of-the-art of experimental techniques. Cell Mol Life Sci 2002; 59:1681-9; PMID:12475179; http://dx.doi.org/10.1007/PL00012496.
30. Alelyunas YW, Pelosi-Kilby L, Turcotte P, Kary MB, Spreen RC. A high throughput dried DMSO LogD lipophilicity measurement based on 96-well shake-flask and atmospheric pressure photoionization mass spectrometry detection. J Chromatogr A 2010; 1217:1950-5; PMID:20153476; http://dx.doi.org/10.1016/j.chroma.2010.01.071.
31. Casimiro M, Rodriguez O, Pootrakul L, Aventian M, Lushina N, Cromelin C, et al. ErbB-2 induces the cyclin D1 gene in prostate epithelial cells in vitro and in vivo. Cancer Res 2007; 67:4364-72; PMID:17483350; http://dx.doi.org/10.1158/0008-5472.CAN-06-1898.
32. Lai EW, Rodriguez OC, Aventian M, Cromelin C, Fricke ST, Martiniova L, et al. ErbB-2 induces bilateral adrenal pheochromocytoma formation in mice. Cell Cycle 2007; 6:1946-50; PMID:17671425; http://dx.doi.org/10.4161/cc.6.15.4521.
33. Rodriguez OC, Lai EW, Vissapragada S, Cromelin C, Avetian M, Salinas P, et al. A reduction in Pten tumor suppressor activity promotes ErbB-2-induced mouse prostate adenocarcinoma formation through the activation of signaling cascades downstream of PDK1. Am J Pathol 2009; 174:2051-60; PMID:19443706; http://dx.doi.org/10.2353/ajpath.2009.080859.
34. Vissapragada S, Ghosh A, Ringer L, Salinas P, Brophy A, Peaceman D, et al. Dietary n-3 polyunsaturated fatty acids fail to reduce prostate tumorigenesis in the PB-ErbB-2 x Pten(+/-) preclinical mouse model. Cell Cycle 2010; 9:1824-9; PMID:20404514; http://dx.doi.org/10.4161/cc.9.9.11542.